Detailed Study of Tröger's Base Separation by SMB Process

Kathleen Mihlbachler
Dept. of Chemistry, University of Tennessee, Knoxville, TN 37996, Division of Chemical Sciences, Oak Ridge National Laboratory, Oak Ridge, TN 37831, and Dept. of Chemical Engineering, O.-v.-Guericke University, Magdeburg, Germany

Andreas Seidel-Morgenstern
Dept. of Chemical Engineering, O.-Guericke University, Magdeburg, Germany

Georges Guiochon
Dept. of Chemistry, University of Tennessee, Knoxville, TN 37996 and Division of Chemical Sciences, Oak Ridge National Laboratory, Oak Ridge, TN 37831

This investigation of the separation of Tröger's base by the SMB process demonstrates: (1) the major importance of a proper modeling of the separation in order to determine the optimal operating conditions; (2) the need of an accurate modeling of the adsorption isotherms of the feed components. The adsorption of Tröger's base onto the stationary phase ChiralPak AD was successfully described by multilayer adsorption isotherm models. Due to the complexity of these models, the region of suitable operating parameters cannot be determined algebraically by the equilibrium theory. As an alternative, the equilibrium-dispersive model, and a reliable numerical algorithm were used to scan a wide operating region, and to define this separation area. To verify the results of these calculations, the separation area was also experimentally detected by performing measurements of product purity and production rate for selected operating points. The combination of a UV detector and a polarimeter allows the accurate monitoring of the internal concentration profiles of both enantiomers. These profiles were compared to the profiles calculated using the multilayer adsorption isotherm models. In addition, the influence of the heterogeneity of the column set on the performance of the SMB process, is studied. Even under strongly nonlinear conditions, excellent agreements between calculated and experimental profiles were obtained. © 2004 American Institute of Chemical Engineers *AIChE J,* 50: 611–624, 2004

Introduction

With sales of enantiomerically pure pharmaceuticals exceeding $100 billion per year (Ahuja, 2000), the pharmaceutical industry is searching for innovative processes to improve the production rate of these compounds. Faced with the FDA's tightened regulation of chiral compounds (FDA, 1992), this industry needs to produce high purity enantiomers. In practice, this need requires considering the implementation of a chromatographic separation process as an alternative, or complement to enantiospecific synthesis. Since the simulated moving bed process (SMB) is essentially a binary separation process, its advantages of being continuous, and of having a low solvent consumption, make it ideal for this application. The most

Correspondence concerning this article should be addressed to G. Guiochon at guiochon@utk.edu.
Current address of K. Mihlbachler: Eli Lilly and Company, Indianapolis, IN; e-mail: mihlbachlerka@lilly.com.

economically promising solution appears now to be in the use of the SMB process applied to the product of an enantioselective synthesis, possibly in combination with crystallization to achieve high enantiomeric purities (Lorenz et al., 2001).

Because a high production rate is important for economical reasons, preparative chromatography must almost always be carried out under nonlinear conditions. The SMB process is complex and numerous parameters must be optimized simultaneously. Multivariate, nonlinear optimization problems can be solved only through numerical calculations. The correct solution of such problems requires proper, sophisticated models of the process, and accurate estimates of the physicochemical characteristics of the system. In the case of SMB, these are the parameters of the adsorption isotherms of the feed components, the column characteristics, and the external dead volumes of the unit. The results of an extensive adsorption isotherm study were previously presented (Mihlbachler, 2002; Mihlbachler et al., 2002b), and of the theoretical and experimental studies of the influence of the heterogeneity of the set of columns onto the SMB process performance (Mihlbachler et al., 2001, 2002a). As shown earlier, it is impossible to pack multiple identical columns (Stanley et al., 1996). In addition, slow changes in the column properties as well as slight temperature or solvent variations might occur during long production runs, or when aggressive solvents are used to clean/disinfect the unit as required by strict regulations. The effects of column variations were also discussed elsewhere (Zhong and Guiochon, 1996; Zenoni et al., 2000). Therefore, the implementation of process control concepts is increasingly studied (Kloppenburg and Gilles, 1999; Wu et al., 1999; Klatt et al., 2000).

The installation of online detectors between two successive columns of the SMB allows the constant monitoring of the internal concentration profiles of the process, and permits immediate response to changing operating conditions. Because chiral compounds are optically active, a combination of a UV-detector and a polarimeter makes possible, in principle, the simultaneous determination of the concentrations of the two enantiomers. However, impurities introduce a degree of complexity. The UV-detector gives a signal that depends on the total concentration of the racemic mixture and of all impurities. The laser polarimeter measures the difference between the concentrations of the two enantiomers, if the impurities are not optically active. If the concentrations of impurities are low, the internal profiles of both enantiomers are readily determined, and their profiles can be compared to the theoretical profiles calculated by various numerical algorithms. The results of this comparison may trigger actions or alarms. Previously, two different systems of online detection at the outlet streams have been reported (Marteau et al., 1995; Zenoni et al., 2000). Although, the main focus of this work is on SMB performance, due to its importance in the separation of racemic mixtures (Azevedo et al., 1999; Pedeferri et al., 1999; Khattabi et al., 2000; Pais et al., 2000), the data acquisition system introduced in this work is suitable for preparative chromatography, with or without closed-loop recycling (Seidel-Morgenstern and Guiochon, 1993b; Blümel et al., 1998; Grill and Miller, 1998; Cherrak et al., 2000), for annular chromatography (Thiele et al., 2001; Uretschläger et al., 2001), as well as for SMB applications with solvent gradients (Antos and Seidel-Morgenstern, 2001), and for simulated moving bed reactors (SMBR) (Fricke et al., 1999; Migliorine et al., 1999; Kawase et al., 2001).

In this work, a systematic approach is illustrated, to optimize an SMB separation in the general case in which the binary isotherms of the feed components do not follow Langmuir isotherm behavior. The first step is the numerical scanning of the entire separation region. This step is the only practical method of determining the separation area when the complex isotherm models of the feed components prevent the use of the analytical methods. In a second step, the separation area is experimentally scanned by choosing several operating points, on the basis of the results calculated. The corresponding experimental internal concentration profiles are obtained by implementing the two-detector system. Calculated and experimental profiles are compared. When they agree, the accuracy of the adsorption isotherm during the operation of the SMB unit will be verified. The use of a complex, but more accurate, adsorption isotherm models allow the optimization for the maximal production rate. In addition, the importance of accounting properly for the differences between the averaged and the exact values of the column porosities are demonstrated. It is shown how the online detector system can identify defective columns within the SMB system through the correct interpretation of changes in the internal concentration profiles, and the outlet concentration histories.

Theory

Equilibrium-dispersive model

For accurate and fast modeling of the SMB process, the most practical model available is the equilibrium-dispersive model (Guiochon et al., 1994; Nicoud and Seidel-Morgenstern, 1996). It assumes instantaneous equilibrium between solid and liquid phases, but a finite column efficiency. Both axial dispersion and the mass-transfer resistances are combined into an apparent dispersion coefficient D_{ap} that is related to the column efficiency under linear conditions, and that is included in the equilibrium-dispersive model. The model assumes that the mass transfers are fast, and it may not account well for cases in which these transfers are slow. This model has been proven accurate in many cases (Guiochon et al., 1994; Seidel-Morgenstern et al., 1998).

In the equilibrium-dispersive model, the differential mass balance for component i in section j, and column k is written

$$\frac{\partial C_{i,j,k}}{\partial t} + u_{j,k}\frac{\partial C_{i,j,k}}{\partial z} - D_{ap}\frac{\partial^2 C_{i,j,k}}{\partial z^2} + F_k\frac{\partial q_{i,j,k}}{\partial t} = 0 \qquad (1)$$

In this equation, the provision of identifying each particular column k in section j is included, while most previous authors assume all the columns to be identical, and merely refer to the columns in section j. This will allow a more precise modeling by including the column characteristics into the chromatographic model (Mihlbachler et al., 2002a). Knowing the exact values of the column porosity ϵ_k, the phase ratio $F_k = (1 - \epsilon_k)/\epsilon_k$, is calculated for each column, and knowing the column efficiency $N_{j,k}$, the apparent dispersion coefficient is given by

$$D_{ap} = \frac{u_{j,k}L_c}{2N_{j,k}} \qquad (2)$$

where the linear velocity of the mobile phase is $u_{j,k}$. Equations 1 and 2 can be solved by the backward-forward finite difference method (Rouchon et al., 1987). To ensure numerical stability in the calculation of the numerical solution, the spatial increments in the column must be adjusted depending on the linear velocity $u_{j,k}$, and the efficiency $N_{j,k}$ (Mihlbachler et al., 2002a). Note that $N_{j,k}$ depends on the velocity through the van-Deemter correlation. Hence, for a given column, it changes when the column moves from a section of the bed to the next.

To solve the mass balance equations for the SMB process, the correct initial and boundary conditions must be defined (Ruthven and Ching, 1989; Storti et al., 1993; Zhong and Guiochon, 1996).

Adsorption isotherm equation

The competitive adsorption behavior of the Tröger's base enantiomers onto Chiralpak AD with 2-propanol as the mobile phase, was found to be nearly unique (Mihlbachler, 2002; Mihlbachler et al., 2002b). It is characterized by an S-shaped isotherm for the more retained (−)-enantiomer, and a negligible influence of the concentration of the less retained (+)-enantiomer on the amount of (−)-enantiomer adsorbed at equilibrium. On the other hand, the pure (+)-enantiomer exhibits Langmuir adsorption behavior, but its concentration in the solid-phase at equilibrium with a given concentration in the mobile phase increases with increasing concentration of (−)-enantiomer. This cooperative interaction is very unusual, competitive behavior being the general rule. Our experimental results are best described by assuming multilayer adsorption with a relatively high degree of (−)-adsorbate-(+)-adsorbate association on the surface of the stationary phase. The isotherm model is based on statistical thermodynamics (Hill, 1960; Lin et al., 1989) describing the formation of multiple layers on the surface of the stationary phase during the adsorption process. The binary (that is, competitive) isotherms are described by the following general equation

$$q_i = \frac{q_s C_i \dfrac{\partial P(C_1, C_2)}{\partial C_i}}{P(C_1, C_2)} \quad i = 1, 2 \tag{3}$$

where $P(C_1, C_2)$ is a polynomial of degree n, and $[\partial P(C_1, C_2)/\partial C_i]$ is its first partial derivative with respect to C_i. A common saturation capacity q_s for both enantiomers is assumed in order to obtain thermodynamically consistent isotherms.

The Langmuir and the quadratic isotherm models describe the formation of monolayer and two-layer adsorption, and, thus, correspond to the first and second order polynomials, respectively. As shown in previous publications (Mihlbachler et al., 2002a, 2002b), these two models are not able to describe the adsorption behavior of Tröger's base accurately. Therefore, a three-layer model was proposed. This more complex model is explained in detail elsewhere (Mihlbachler, 2002; Mihlbachler et al., 2002b). Here, only the final function $P(C_1, C_2)$ is shown

$$P = 1 + b_1 C_1 + b_2 C_2 + b_{11} C_1^2 + b_{22} C_2^2 + (b_{21} + b_{12}) C_1 C_2 + b_{211} C_1^2 C_2 \tag{4}$$

Experimental results suggested (Mihlbachler et al., 2002b) that, if there is competition or cooperation for adsorption of the more retained enantiomer, its contribution is too small to have significant influence. To account for the S-shape adsorption behavior of the more retained compound, its isotherm model is reduced to a noncompetitive quadratic model. The set of binary isotherms used in this article is as follows

$$q_1 = q_s C_1 \frac{b_1 + 2b_{11} C_1 + b_{12} C_2 + b_{21} C_2 + 2b_{211} C_2 C_1}{P} \tag{5}$$

$$q_2 = q_s C_2 \frac{(b_2 + 2b_{22} C_2)}{1 + b_2 C_2 + b_{22} C_2^2} \tag{6}$$

Detailed information regarding the comparison between the isotherm models proposed in Eqs. 5 and 6, and the experimental data are given elsewhere (Mihlbachler, 2002; Mihlbachler et al., 2002b).

Revised set of separation conditions

The SMB process can be described as an equivalent true moving bed (TMB) process (Ruthven and Ching, 1989). On the basis of adsorption behaviors of both compounds, the proper separation conditions of the SMB process are defined. The SMB unit is divided into four sections with one or more columns per section. Between the sections are alternating inlet and outlet valves for the feed or solvent streams, and for the extract or raffinate streams, respectively. To simulate the movement of the solid phase of the TMB process, the valve positions are switched in the fluid flow direction. The more retained compound is more strongly adsorbed to the stationary phase and, therefore, moves to the extract outlet; and the less retained compound is already eluted into the liquid phase and moves to raffinate outlet. The flow rates Q_j in all four sections of the SMB unit must guarantee that the positions of each of the fronts and rears of the concentration profiles of the two compounds are within a certain range before the next switching occurs (see Eqs. 9–11 and Eqs. 12–14, as definitions of the boundary conditions). The flow rates in section II and III of the SMB unit effect the performance of the separation. In section II, between extract and feed-valves, the less retained compound is desorbed, but the more retained compound remains adsorbed onto the solid-phase. The adsorption front of the more retained compound in section III is not allowed to pass the raffinate outlet valve, whereas the less adsorbed compound migrates with a high concentration into the fourth section. In addition, the flow rate in section IV hinders the breakthrough into section I. In section I, the solid-phase is regenerated by desorbing the more retained compound. The length of the switching period is dependent on the solid-flow rate of the TMB process

$$Q_S = (1 - \epsilon_k) A u_s = (1 - \epsilon_k) A L_C / t^* \tag{7}$$

where t^* is the switching (or cycle) time, u_s is the apparent velocity of the solid-phase, ϵ_k in the porosity of column k, and A is the cross section area of the column. In applying the equilibrium theory (Ruthven and Ching, 1989; Storti et al., 1989), that is, assuming infinite column efficiency, and no influence of axial dispersion and mass-transfer effects, the

separation conditions are derived. To simplify the modeling, the solid-phase flow rates and void fractions of all columns are set constant.

Previously, the authors accounted for heterogenous column characteristics, in particular variations of the porosity values of a column set, by implementing a revised set of separation conditions (Mihlbachler et al., 2001). However, when the columns ($k = 1, \ldots, n$) of an SMB set have different properties, the true period of the system, that is, the time after which the system returns to its initial condition, is no longer the switching, time but it is n times larger. This time is referred to as the superperiod of the SMB.

According to the equilibrium theory and the so-called "Triangle theory" (Ruthven and Ching, 1989; Storti et al., 1989), the dimensionless internal flow rate ratios are defined as

$$r_j = \frac{Q_j t^*}{AL_C} \tag{8}$$

These flow rate ratios do not depend on the column porosities. By contrast, the following boundary parameters consider the column porosities

$$a^*_{1,k} = a_1(1 - \epsilon_k) + \epsilon_k \tag{9}$$

$$a^*_{2,k} = a_2(1 - \epsilon_k) + \epsilon_k \tag{10}$$

In these equations, the subscript k identifies the physical column. A simple algebraic transformation (Mihlbachler et al., 2001) leads to the following new set of equations under linear conditions

$$r_{IV} \le a^*_{1,k} \le r_{II} \le r_{III} \le a^*_{2,k} \le r_I \tag{11}$$

The revised set of separation conditions (Eq. 11) is extended to nonlinear SMB operation. On the basis of the "Triangle theory" (Storti et al., 1989, 1993), the separation area for Langmuirian adsorption-isotherm behavior is defined by accounting for the differences in the column porosities

$$a^*_{2k} < r_I < \infty \tag{12}$$

$$r_{II,cr}(r_{II}, r_{III}) < r_{II} < r_{III} < r_{III,cr}(r_{II}, r_{III}) \tag{13}$$

$$0 < r_{IV} < r_{IV,cr} = \epsilon_k + \frac{(1 - \epsilon_k)}{2}\{a^*_{1k} + r_{III} + b_1 c_{\text{feed},1}(r_{III} - r_{II}) - \sqrt{[a^*_{1k} + r_{III} + b_1 c_{\text{feed},1}(r_{III} - r_{II})]^2 - 4a_1 r_{III}}\} \tag{14}$$

The lower boundary of r_{IV} is set to zero, due to the negligible value of ϵ_p.

The "Triangle theory" cannot be easily extended to anti-Langmuirian adsorption behavior, due to the fact that the ideal equilibrium model is only solvable algebraically under the limited circumstances of a few simple adsorption isotherm models (Guiochon et al., 1994). More complex isotherm models must be solved numerically. As an alternative, the reliable numerical algorithm described in the subsection Equilibrium-dispersive model (p. 2) is used to scan a wide region, and to determine the separation area (Seidel-Morgenstern et al., 1998; Kniep et al., 2000). The shape of this area is related to the applied isotherm models as well as to the column characteristics.

Experimental Settings

The racemic mixture of Tröger's base (Aldrich, Milwaukee, WI) with a total concentration of 7 g/L, was separated using chromatographic columns packed with Chiralpak AD (approximately 4.5 g per column) from Chiral Technologies (Exton, PA). This packing material consists of a porous silica gel coated with amylose tri-(3,5-dimethyl carbamate). The particle size is 20 μm. The stainless steel columns used in the experiments had an inner diameter of 1 cm, and were 10 cm long. The mobile phase was pure HPLC-grade 2-propanol from Fisher Scientific (Pittsburgh, PA). The feed concentration was chosen below the solubility of the racemic mixture, to avoid possible crystallization within the chromatographic system.

A laboratory-scale SMB unit (ICLC 16-10) from Prochrom (now Novasep, France), was used in an eight-column configuration (two columns per section). Five 16-port pneumatically-actuated valves (Valco, Houston, TX) realized the continuous operation of the SMB process by switching the column position of the two inlet streams (solvent and feed), and the three outlet streams (extract, raffinate, and recycle). Constant flow rates in the four sections were maintained using four HP 1050 pumps (Agilent Technologies, Palo Alto, CA).

Two Spectroflow UV detectors (Model 757 from Perkin Elmer, Forster City, CA) monitored the composition of the extract and the raffinate outlet streams. A HP 1100 UV detector (Agilent Technologies) with a high-pressure flow cell and a laser polarimeter (PDR-Chiral, Palm Beach Gardens, FL), were installed within the flow cycle of the SMB system, at the outlet of one of the columns. The experimental data from these four detectors were recorded using LabView (National Instruments, Austin, TX), a program installed on an additional computer. More detailed information such as regarding the calculation of the internal concentration profiles of each of the two enantiomers, are given elsewhere (Mihlbachler, 2002; Mihlbachler et al., 2002a).

The column characteristics and adsorption isotherm parameters were determined by an HP 1090 liquid chromatograph (Agilent Technologies, Palo Alto, CA). This instrument was equipped with a high-pressure flow cell (up to 400 bar) and diode array, multiple wavelength detector. The procedure of the adsorption isotherm determination are extensively explained elsewhere (Mihlbachler et al., 2002b).

Results and Discussion

Chromatographic system parameters

To perform this detailed study of an enantioseparation by SMB chromatography, the essential system parameters must be determined. First, the chromatographic columns of the SMB system were characterized. These experiments were performed at a flow rate of 1 mL/min. In Table 1 the porosities ϵ_k of all columns, measured from the retention time of a nonretained compound (1,3,5-tri-tert-butylbenzene), are listed. The column **c04**, which has a porosity equal to the average porosity of the

Table 1. Characteristic Parameters of The Columns Used

Column	Position within SMB	Porosity ϵ_k
*c*04*		0.648
*c*14	7	0.654
*c*11	5	0.651
*c*12	6	0.650
*c*13	8	0.651
*c*09	4	0.645
*c*05	2	0.645
*c*02	1	0.643
*c*08	3	0.642
Average value		0.648
RSD (%)		0.7
"defect"	6**	0.619

*Column used in the HP1090 system from Agilent to determined the adsorption isotherm parameters and the purity values of the outlet streams.
**Column in position 6 was exchanged.

columns in the SMB set, was used for the determination of the adsorption isotherm data, and for the determination of the parameters of the isotherm model. From the retention times of the components of an analytical amount of the racemic mixture, the values of the Henry coefficients can be derived, with $a_1 = 1.679$ and $a_2 = 3.426$. These coefficients give the initial slopes of the isotherms. The separation factor of 2.04 indicates a relative easy separation. The column efficiency of 1,270 theoretical plates is relatively high for the nonretained compound. For the lesser, and the more retained enantiomers, the number of theoretical plates are smaller, with estimates of 560 and 420 plates, respectively (Mihlbachler, 2002).

The Langmuir isotherm model generally used in the design of the SMB process are not valid for the modeling of overloaded elution chromatography of the Tröger's base enantiomers (Seidel-Morgenstern and Guiochon, 1993a; Mihlbachler et al., 2002b). As a consequence, this model also fails to account for their behavior in the more complicated SMB process. The unique adsorption behavior of the racemic mixture was determined from results obtained with the perturbation method. It was shown that this method was superior in accuracy over frontal analysis in the case in point, because of the presence of impurities in the samples available (Mihlbachler et al., 2002b). In Table 2, the parameters of the different isotherm models to which the data were fitted, are summarized. These models include two Langmuir models, one model with the set Henry coefficients, and the other obtained as the best-fit model, and the three-layer model (see Eqs. 5 and 6). The accuracy of the last model was verified elsewhere (Mihlbachler et al., 2002b).

Determination of separation area and operating points

The separation area of the SMB system in the r_{II}–r_{III} plane must be defined for finding operating conditions for the separation that are both optimal and robust. An algebraic solution can be obtained when the adsorption data are correctly accounted for by the Langmuir model. When this isotherm model is not applicable, as in our case, this solution is not valid, and may even be grossly incorrect, as shown later. Since there is no algebraic solution, the entire region was numerically scanned by calculating the solution of the mass balance equations of the separation (Eq. 1) for a dense network of points representing possible combinations of experimental conditions. The results obtained with the three-layer isotherm model are displayed in Figure 1, together with those obtained with the two Langmuir models (see Table 2). Five different operating points (★), along a straight line parallel to the diagonal of the r_{II}–r_{III} plane, represent the experimental conditions used for an experimental scanning of the separation area. These points were arbitrarily chosen, but should represent the possible separation area, with special focus on the boundaries of this area.

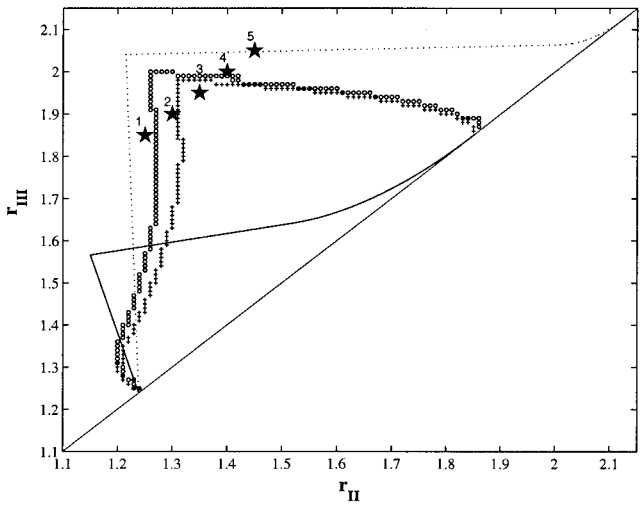

Figure 1. Separation area for C_{Feed}.

+—Calculated by the three-layer isotherm model with 8 exact porosity values *, **o**—calculated by the model with the averaged porosity value *, dotted line—best-fit Langmuir model **, solid line—Langmuir model with a set of Henry coefficients **, and ★—five operating points (see Table 3). *: N = 150 and purities of extract and raffinate streams > 98%. **: Analytical solution of "Triangle theory."

The separation areas in Figure 1 were calculated with the three-layer adsorption isotherm model in two different ways. First, the exact porosity values of each column were used (+). Then, the average porosity value for the column set was used (**o**). The concentrations of both enantiomers at each outlet were averaged over one superperiod, when the exact porosity values were applied. For the numerical calculations of the two separation areas, the purity values of the extract and raffinate stream were set at 98% or better. The calculations were performed, assuming 150 theoretical plates per column. This number was experimentally estimated from an overloaded elution profile through all SMB columns. The extracolumn volumes (less than 5% per column volume in our case), diffusion, and mass-

Table 2. Adsorption Isotherm Parameters Determined by the Perturbation Method

Model	q_s [g/l]	b_1 [l/g]	b_2 [l/g]	b_{11} [l^2/g^2]	b_{22} [l^2/g^2]	b_{21} [l^2/g^2]	b_{221} [l^3/g^3]	SD
Langmuir with set Henry coefficients	54	0.0311	0.0635					0.610
Best-fit Langmuir	313.96	0.00048	0.01214					0.608
Three-layer	28.25	0.0595	0.1212	0.000549	0.0139	0.0027	0.00083	0.258

Table 3. Operating Points of the SMB Experiments

op	Q_1 [mL/min]	Q_2 [mL/min]	Q_3 [mL/min]	Q_4 [mL/min]	Q_{ex} [mL/min]	Q_f [mL/min]	Q_{ra} [mL/min]	t^* [s]	r_1	r_2	r_3	r_4
bp125185	1.05	0.63	0.93	0.60	0.42	0.30	0.33	940	2.10	1.25	1.85	1.20
bp1319	1.05	0.65	0.95	0.60	0.40	0.30	0.35	940	2.10	1.30	1.90	1.20
bp135195	1.05	0.68	0.98	0.60	0.37	0.30	0.38	940	2.10	1.35	1.95	1.20
bp142	1.05	0.70	1.00	0.60	0.35	0.30	0.40	940	2.10	1.40	2.00	1.20
bp145205	1.05	0.73	1.03	0.60	0.32	0.30	0.43	940	2.10	1.45	2.05	1.20
op	1.05	0.66	0.93	0.60	0.39	0.27	0.33	924	2.06	1.30	1.83	1.18

transfer effects within the SMB unit reduce the efficiency of the columns significantly (Mihlbachler, 2002). The solid and dashed lines are the analytical solutions of the "Triangle theory" for the two Langmuir isotherms, the one obtained with the Henry coefficients derived from an analytical chromatogram, and the best-fit competitive Langmuir model, respectively.

Table 3 lists the flow rate ratios r_j, and the corresponding flow rates Q_j in each section j of the SMB process, and the flow rates of the inlet and outlet streams (Q_{feed}, Q_{ex}, and Q_{ra}) corresponding to each operating point in Figure 1. These points are within the separation triangle, calculated by the best-fit Langmuir isotherm model.

Comparing the shapes of the separation areas in Figure 1 confirms the considerable importance of an accurate modeling of the isotherm, when the use of computer assisted optimization is contemplated. The available area of separation shrinks significantly compared to the one afforded by the triangle derived from the best-fit Langmuir isotherm, and its border is quite different. By contrast, the area of separation actually available is far larger than the one predicted on the basis of the best Langmuir isotherm derived, using the Henry coefficients measured from analytical data (Figure 1). This figure also illustrates how the true separation area, the one calculated with the true column porosities, is narrower than the one derived from the average porosity of the column set.

Only the use of an accurate, if sophisticate, isotherm model, gives correct calculated separation conditions that allow a high production rate and guarantee the purity of the products. It should be understood that no short-cuts are acceptable, and that isotherm accuracy is the required condition for obtaining reliable optimized conditions. The case is further illustrated by the considerable difference between the separation areas corresponding to the two Langmuir models, in spite of the fact that the coefficients of these models are derived from the experimental data acquired, using frontal analysis and the perturbation method, methods that are both rather popular. However, these isotherms are both inaccurate, because the accurate isotherm data were fitted to wrong isotherm models.

Experimental verification of the adsorption isotherm model

In the following subsections the accuracy of the adsorption isotherm models previously selected for describing the adsorption behavior of the Tröger's base enantiomers, is assessed by comparing the experimental and calculated internal concentration profiles measured in the SMB unit. The combination of the online UV- and polarimetric detection allows the calculation of the concentration profiles of both components during the separation of the racemic mixture. This provides the most precise information regarding the separation process. This information is particularly important in the case of nonconventional adsorption behavior, such as the one of Tröger's base onto the CSP used in this work (it appears that "conventional," that is, Langmuirian, adsorption behavior tends to be rarer than the unconventional one in chiral separations (Fornstedt et al., 1998)). An experimental scanning of the separation area was carried out by selecting operating points (see Figure 1 and Table 3). The switching time and the feed flow rates were kept constant for all these operating points. Their low values were selected to reduce the influence of the column switching on the baseline of the polarimeter signal. The primary goal of this research had not been the search for the maximal production rate. The extra column volumes within the SMB unit were taken into account in the calculation of the values of the switching time, as explained elsewhere (Migliorine et al., 1999; Mihlbachler, 2002).

The internal concentration profiles that had been experimentally determined were compared to the profiles calculated with the three-layer isotherm model, using the average column porosity. In the following figures, the experimental profiles are the lines. The profiles calculated with the three-layer adsorption isotherm model are those identified by the symbol ★. All the calculations were performed assuming a column efficiency of 150 theoretical plates. The experimental values were determined carefully. The influence of the impurities present were neglected. However, besides the unavoidable experimental errors, the values obtained are somewhat influenced by the presence of these impurities. For example, the purity of the outlet streams cannot be quantified because the detector response for the (unknown) impurities in the Tröger's base samples could not be calibrated. All the experimental and calculated values of the purities and production rates of both outlet streams, and the corresponding statistical values, are listed elsewhere (Mihlbachler, 2002). Selected values only are reported here.

As a first example, the operating point op5 in Table 3 is examined due to its position at the upper border of the separation area. At this condition, the separation is less robust, and the raffinate outlet stream is slightly polluted. Only one set of experimental concentration profiles recorded during one superperiod at the outlet of column No. 6 is compared to the calculated profiles in Figure 2. The influence of the accumulated impurities on the response of the UV-detector, and the separation in general should be noted. It explains, for example, the step on the raffinate rear and the one on the front of the extract profile. Allowing for this effect, there is a good general agreement between experimental and calculated results, even in this difficult case. It appears that the experimental profile of the raffinate moves more slowly, and is more concentrated than the one calculated. Also, the rear front of the experimental profile of the extract drifts faster in the solid-phase direction

than the one calculated. The front of the raffinate moves faster in section IV if calculated using the three-layer model (★). In spite of these problems, there is an excellent agreement between experimental and calculated product purities (Figure 3).

The influence of the accumulated impurities on the recorded signal can be reduced when only the polarimeter signals are compared to the results of the calculations (see Figure 4). A better agreement between the experimental and calculated concentrations profiles of the two enantiomers is then reached, particularly for the less retained enantiomer. The cyclic behavior of the SMB process, and the oscillations occurring during a superperiod are accurately described by the calculations. Also, the behavior in the middle sections of the process is well characterized by the adsorption isotherm model. Nevertheless, the timing of the experimental and calculated concentration fronts are different. At least in large part, this is caused by not considering the adsorption behavior of the accumulated impurities, and by the inaccurate inclusion of the extra-column volumes. In particular, the concentration front of the less retained enantiomer calculated by the three-layer isotherm model moves significantly faster than the experimental front within sections III and IV. It is also less steep. On the basis of the isotherm model (Eq. 5), the retention time of the less retained enantiomer increases in the presence of the more retained compound. During the *ideal* computer simulation, the extract is not always present in these sections. The less retained the compound is the less strongly adsorbed, and thus, moves faster, which explains the difference between the positions of the raffinate fronts. It is worth noting that the experimental concentration profiles recorded at the outlet of four different columns of the set are different. For an ideal process, these profiles

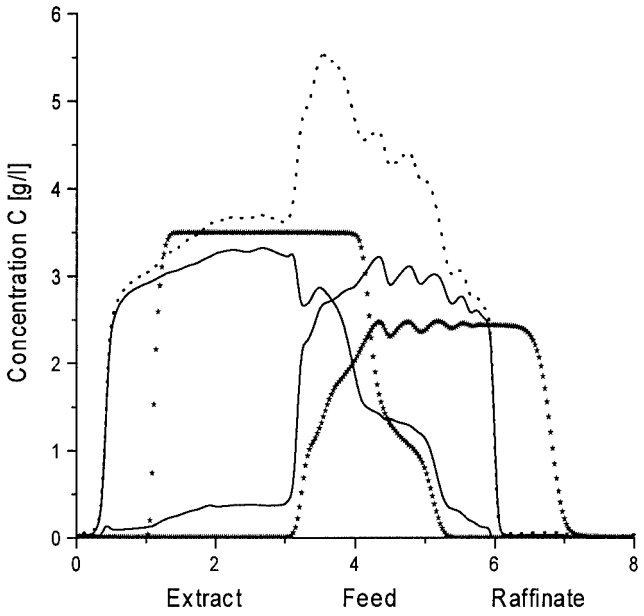

Figure 2. Experimental and calculated internal concentration profiles at the operating point op5 (Table 3).

Dashed line—experimental profile of the racemic mixture at column outlet 6, solid line—experimental profile of the single compounds at column outlet 6, and ★—calculated profiles of the single compounds with three-layer isotherm model (Eqs. 5 and 6) and $\epsilon_{av} = 0.648$.

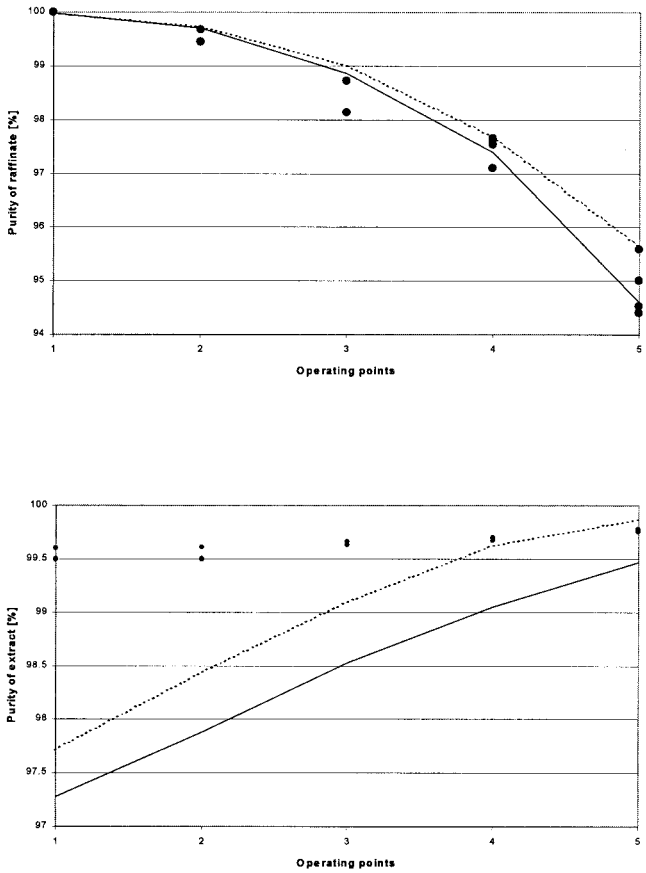

Figure 3. Comparison between experimental and calculated raffinate, and extract purities for operating points op1–5 (Table 3).

(●)—Experimental data, solid line—averaged purity calculated with exact porosities (Table 1) and three-layer model (Eqs. 5 and 6), and dotted line—purity calculated with average porosity ($\epsilon_{av} = 0.648$) and three-layer model.

in Figure 4 should be identical. Profile variations happen because the nature of the SMB process is complex, and the column set is heterogeneous.

Although significant differences in the internal concentration profiles were observed, the differences between the calculated and experimentally determined purities of the raffinate are not important. As shown in Figure 3, the isotherm model gives calculated values of the product purity that agree within one percent with the values measured in the experiment. The largest RSD value for the raffinate purity, calculated for all the experimental runs, and for the value calculated using the average column porosity, and the three-layer model (see Table 4), is only 0.92%. More detailed information can be found elsewhere (Mihlbachler, 2002). The differences between the values obtained for the extract purity are not significant either. In addition, the differences between experimental and calculated production rates is shown in Table 4. For example, the maximum differences between the experimental production rates of the extract and raffinate streams, and those calculated with the three-layer model have an RSD of 9.25% and 4.7%, respectively. Nevertheless, the accuracy of the calculated production rates compared to the experimental values is surprisingly good.

To reduce the influence of the impurities on the comparison

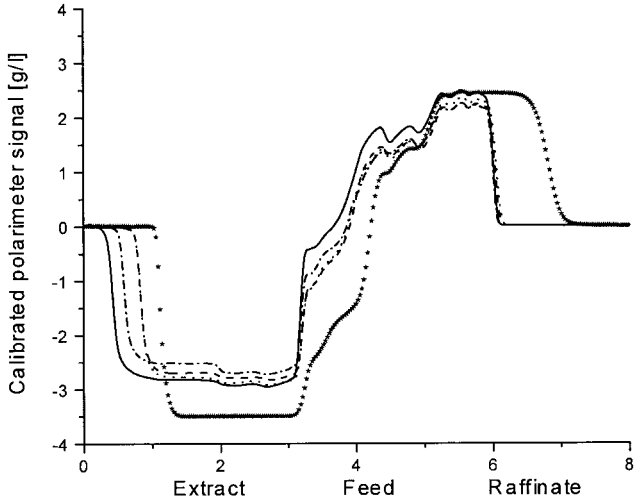

Figure 4. Experimental and calculated internal concentration profiles detected by the polarimeter at the operating point op5 (Table 3).

Solid line—experimental at column outlet 6, dotted line—at position 5, dash-dotted line—at position 7, dashed line—at position 8, and ★—calculated with three-layer isotherm model (Eqs. 5 and 6) and $\epsilon_{av} = 0.648$.

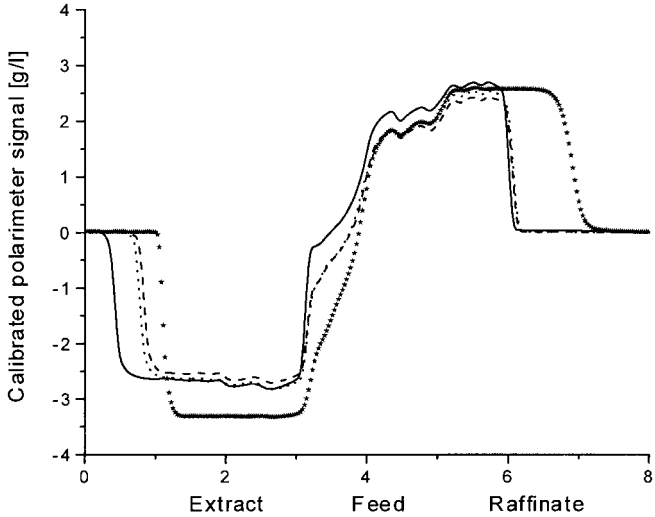

Figure 5. Experimental and calculated internal concentration profiles detected by the polarimeter at the operating point op4 (Table 3).

Solid line—experimental at column outlet 5, dotted line—at position 6, dashed line—at position 8, and ★—calculated with three-layer isotherm model (Eqs. 5 and 6) and $\epsilon_{av} = 0.648$.

of the internal concentration profiles, only the profiles recorded by the polarimeter are used in reporting the data obtained for the other operating points. For the next three operating points (op4, op3, and op2 in Table 3), the agreement between the calculations made with the model and the experimental profiles decreases despite the fact that these points are deeper within the robust region of the separation area (Figures 5–7). The differences between the purity values derived from the experimental samples and those calculated increase, as shown in Figure 3. However, the purity of the extract stream decreases slightly, while that of the raffinate stream improves with declining *r*-values (see Table 3).

In Figure 8, the three-layer model (★) accurately describes the adsorption behavior at operation point op1, during the SMB separation. The raffinate stream is pure in both the experimental and the calculated concentration histories (see Figure 3).

Table 4. Purity and Productivity of the Extract and Raffinate Streams Experimentally Determined and Calculated with the Three-layer Models for the Operating Point op5

	Purity (%)		Productivity g/day/kg$_{pack}$	
	Extract	Raffinate	Extract	Raffinate
Exp. data				
Col. outlet 5	99.75	95.59	35.14	40.03
Col. outlet 6	99.78	94.52	34.72	38.59
Col. outlet 7	99.77	95.00	34.14	38.65
Col. outlet 8	99.78	94.40	34.93	38.81
Cal. A*	99.47	94.60	38.33	40.98
RSD (%)	0.22	0.74	8.18	4.25
Cal. B**	99.87	95.64	38.91	41.25
RSD (%)	0.09	0.92	9.25	4.70

RSD = Relative standard deviation between experimental and calculated data.
A* = Averaged value calculated with porosity values ϵ_i.
B** = Value calculated with average porosity ϵ_{av}.

The too high pollution of the extract stream (see Figure 3 and Table 5), obtained with the calculation results from the breakthrough of the raffinate stream from section IV into section I. The switching time is too short to allow complete bed regeneration in section IV. This breakthrough does not occur under experimental conditions because the adsorption of the less retained enantiomer is actually somewhat less strong than predicted. The difference in the purity values of the extract stream is only 1.35% (see Table 5). This difference may be caused by the impurity accumulating within the SMB process

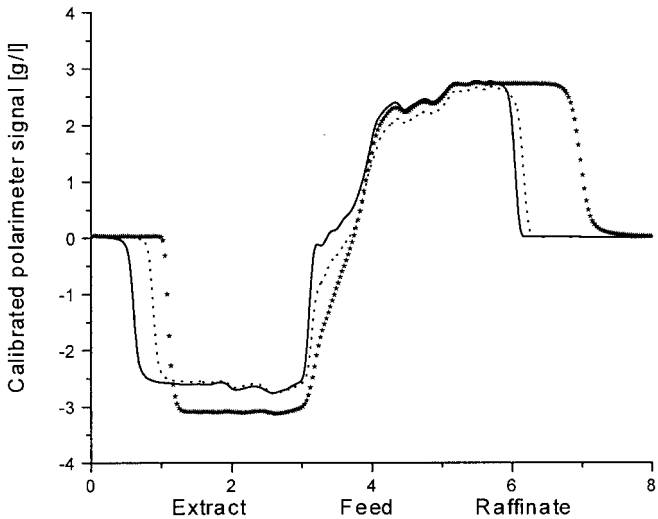

Figure 6. Experimental and calculated internal concentration profiles detected by the polarimeter at the operating point op3 (Table 3).

Solid line—experimental at column outlet 6, dotted line—at position 5, and ★—calculated with three-layer isotherm model (Eqs. 5 and 6) and $\epsilon_{av} = 0.648$.

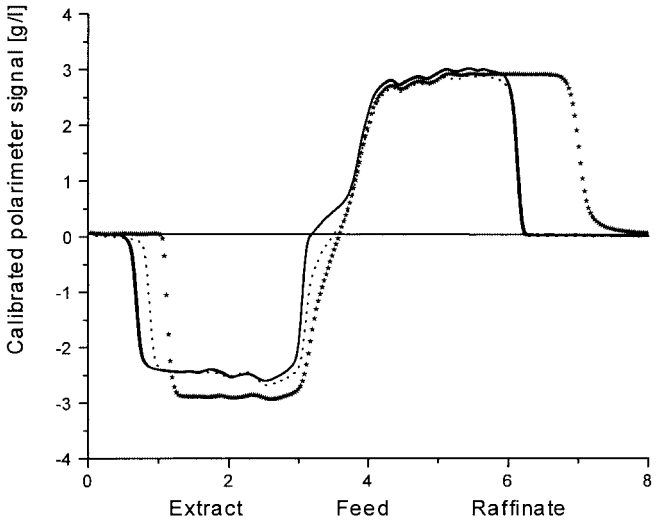

Figure 7. Experimental and calculated internal concentration profiles detected by the polarimeter at the operating point op2 (Table 3).

Solid line—experimental at column outlet 6, dotted line—at position 5, and ★—calculated with three-layer isotherm model (Eqs. 5 and 6) and $\epsilon_{av} = 0.648$.

as shown in Figure 9. The impurities are achiral and can only be detected by the UV-detector.

It is worth noticing the excellent agreement of the cyclic behavior of the SMB process (that is, the correct prediction of the oscillations of the internal concentration profiles) for all operating points.

When comparing the production rates corresponding to all the operation points along the parallel to the diagonal of the separation area, it was found that the calculated values increase with increasing r_{II} and r_{III} for the raffinate, and, thus, decrease

Table 5. Purity and Productivity of the Extract and Raffinate Streams Experimentally Determined and Calculated with the Three-layer Models for the Operating Point op1

	Purity (%)		Productivity g/day/kg$_{pack}$	
	Extract	Raffinate	Extract	Raffinate
Exp. data				
Col. outlet 5	99.50	100	39.23	38.44
Col. outlet 6	99.60	100	39.44	39.18
Cal. A*	97.28	99.98	41.41	39.98
RSD (%)	1.67	0.01	3.82	2.78
Cal. B**	97.72	99.99	41.36	40.29
RSD (%)	1.35	0.01	3.73	3.34

RSD = Relative standard deviation between experimental and calculated data.
A* = Averaged value calculated with porosity values ϵ_i.
B** = Value calculated with average porosity ϵ_{av}.

for the extract. This result is consistent with the purity values. Although the experimental results indicate a similar tendency, the differences between calculated and experimental values vary differently. Wider variations can be seen at the border of the separation area, which can be caused by several reasons, such as the presence of impurities, experimental errors, errors in the adsorption model, and the influence of the heterogeneity of the SMB system.

Effect of the heterogeneity of the column set on the performance of the SMB process

As shown in Figures 4–8, the positions of the adsorption and desorption fronts of the internal concentration profiles vary when recorded at different column outlet positions. Also, the values of the extract and raffinate purities as well as their production rates change depending on the outlet position where the outlet streams are collected. The values are listed in Tables 4–6 and elsewhere (Mihlbachler, 2002). Due to the complexity

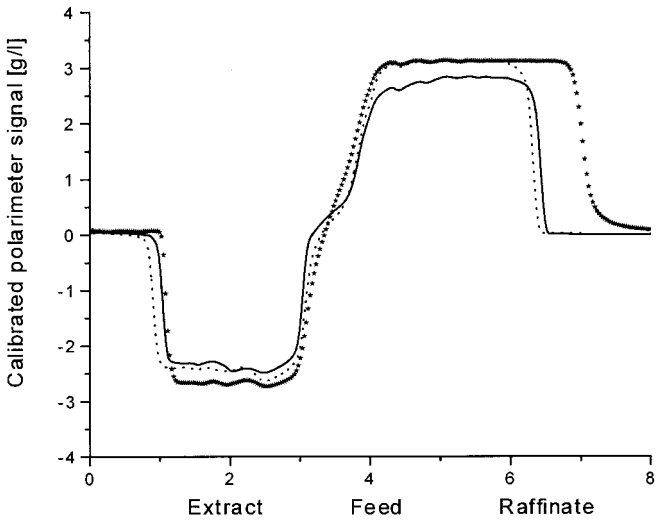

Figure 8. Experimental and calculated internal concentration profiles detected by the polarimeter at the operating point op1 (Table 3).

Solid line—experimental at column outlet 6, dotted line—at position 5, and ★—calculated with three-layer isotherm model (Eqs. 5 and 6) and $\epsilon_{av} = 0.648$.

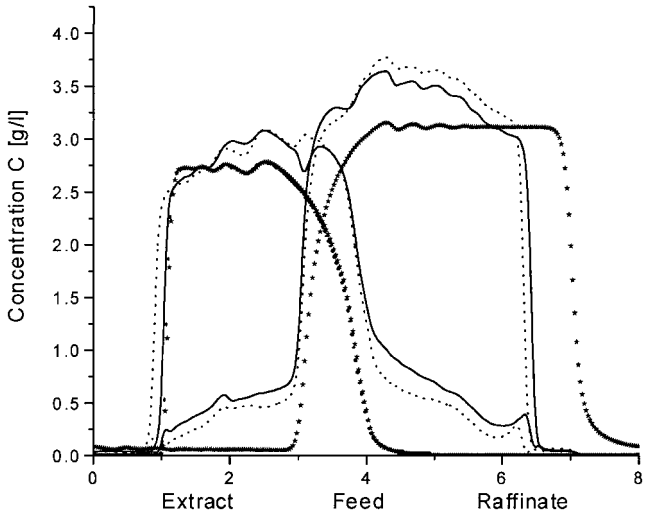

Figure 9. Experimental and calculated internal concentration profiles of the single compounds at the operating point op1 (Table 3).

Solid line—experimental at column outlet 6, dotted line—at position 5, and ★—calculated with three-layer isotherm model (Eqs. 5 and 6) and $\epsilon_{av} = 0.648$.

Table 6. Purity of the Raffinate Streams Experimentally Determined and Calculated with the Three-Layer Models for the Operating Point op4

	Raffinate Purity, %		
	Exp. Data	Three-layer	*RSD*, %
Col. outlet 5	97.62	97.48	0.10
Col. outlet 6	97.10	97.52	0.31
Col. outlet 7	97.66	97.57	0.07
Col. outlet 8	97.55	97.44	0.08
Cal. A*		97.40	
RSD (%)		0.30	
Cal. B**		97.69	
RSD (%)		0.59	

RSD = Relative sum of the squares of the residuals between experimental and calculated data.
A* = Averaged value calculated with porosity values ϵ_i.
B** = Value calculated with average porosity ϵ_{av}.

of the SMB process, many different parameters combine causing these differences, but that cannot be due to the extra-column volume introduced with the detector cell, and which disturbs the "ideal" internal profiles. If the online detector system were installed at a different outlet position, it would cause an identical disturbance to the "ideal" separation process, and, thus, the measured internal profiles would remain unchanged. Hence, other parameters, such as the heterogeneity of the column set, influence the performance of the separation. Here, only the effects of variation in the column porosity were examined.

The values of the product purity and the production rate, calculated with the average column porosity ($\epsilon_{av} = 0.648$), are listed for the operating points 5, 1 and 4, in Tables 4–6, respectively, as well as the average values of these properties calculated with the exact column porosity values (see Table 1). Depending on where the operating point lies in the separation area, and at which column position the outlet streams are collected, the values of the purity and productivity vary. All the values were determined experimentally, those calculated, and the corresponding statistical values are listed elsewhere (Mihlbachler, 2002).

As an example, the operating point op4 was chosen for a further study of the influence of the column porosity on the performance of the SMB process. This operating point is located on the upper border of the separation area (Figure 1). To verify the repeatability of the experimental performance, the two profiles are recorded at the outlet of the column in position six at eight months distance, as shown in Figure 10. These experimental profiles are also compared with the profiles calculated by the three-layer (symbol ★) adsorption isotherm models, and using either the average (filled symbol) or the exact (open symbol) column porosity values.

First, there is an excellent reproducibility of the experimental profiles. The two experiments were made at eight months distance, hence, at different seasons, but in a climate-controlled laboratory, at a nearly constant temperature of approximately 25°C. The different calculated profiles exhibit some differences in the front positions of the raffinate in section IV, depending on the value of the porosity used. The fronts calculated with the exact porosity move faster. The profiles recorded experimentally, are more retained than the calculated ones.

In Table 6, all the values measured experimentally for the

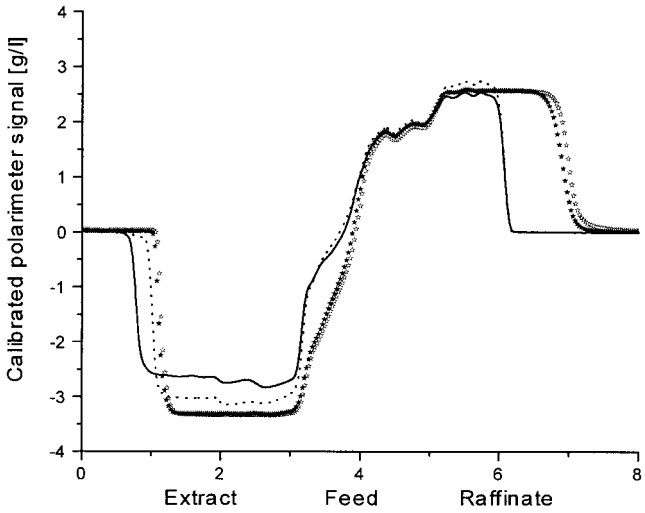

Figure 10. Repeatability of internal concentration profiles detected by the polarimeter at the operating point op4 (Table 3).

Solid line—experimental at column outlet 6, dotted line—recorded at outlet 6 during prior testing, and ★—calculated with three-layer isotherm models (Eqs. 5 and 6): filled symbol—with $\epsilon_{av} = 0.648$, and open symbols with exact porosity values at position 6.

raffinate purity are listed and compared to the values calculated. It is clear, an oscillation of the purity values can be observed. Similar results are observed for the extract purities. Because of the position of this operating point in the separation triangle, the extract stream is almost pure, at 99% or better, as already shown in Figure 3. The raffinate purity varies between 97% and 98%.

In Figure 11 a comparison between the experimental con-

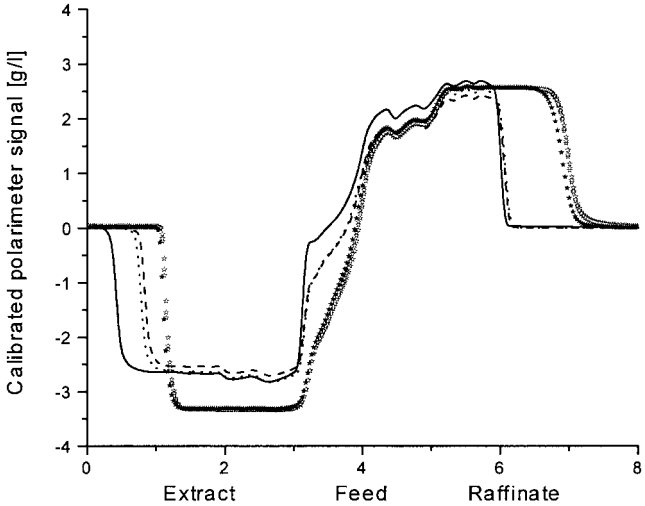

Figure 11. Internal concentration profiles detected by the polarimeter, and calculated by three-layer model (Eqs. 5 and 6) at the operating point op4 (Table 3).

Solid line—experimental at column outlet 5, dotted line—at position 6, dashed line—at position 8, ★—calculated with three-layer isotherm model (Eqs. 5 and 6) and $\epsilon_{av} = 0.648$, and open ★—calculated at positions 5, 6, and 8.

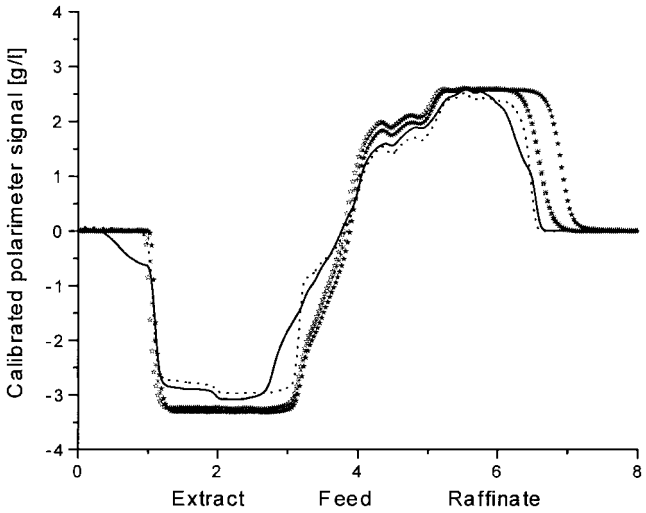

Figure 12. Internal concentration profiles of the column set with a "defective" column at the operating point op4 (Table 3).

Solid line—recorded at the outlet of the "defective" column 6, dotted line—at the outlet of the column in front of the "defective" column 5, ★—calculated with three-layer model (Eqs. 5 and 6) and with average porosity, and * and open ★—calculated with three-layer model with exact porosity values (see Table 1) at positions 5 and 6.

centration profiles monitored at three different positions (5, 6, and 8) within the SMB, and the profiles calculated with the three-layer model (★), is displayed. The front positions vary only slightly in the middle sections and at the raffinate outlet (sections II to IV), but they do so more significantly in section I. The heights of the profiles are slightly different. The cyclic behavior of the SMB process shown as oscillations in the profiles are well reproduced. However, experimental and calculated front positions disagree slightly. It appears that the compounds are more strongly retained than the calculations predict. The difference may be caused by the presence of impurities and their influence on the adsorption behavior of the enantiomers (Mihlbachler et al., 2002b).

Detection of defective columns within the SMB unit

So far reported in this article, replacing one of the chromatographic columns of the SMB set used to collect the results with a "defective" column (that is, a column with $\epsilon = 0.619$), introduces significant changes in the performance of the SMB separation. As an example, Figure 12 displays the experimental profiles recorded at the outlet of the "defective" column, and of the column immediately in front of it, with the SMB being operated under the conditions of point op4. A distinct disturbance of the profile recorded at the outlet of the "defective" column is observed. Comparing these experimental profiles to the calculated profiles, using the three-layer adsorption isotherm model (★) for calculating the SMB separation, also provides excellent agreement (see Figure 12), especially when the exact porosity values are implemented (open ★). The oscillations of the profiles caused by the cyclic behavior of the SMB process are well represented. In Table 7, all the experimental and calculated values of the purity and production rate are summarized (Mihlbachler, 2002). During the experiments,

Table 7. Purity and Productivity of the Extract and Raffinate Streams Experimentally Determined and Calculated with the Three-Layer Models for the Operating Point op4 with the "Defective" Column in Position 6 of the SMB System (see Table 1)

	Purity (%)		Productivity g/day/kg$_{pack}$	
	Extract	Raffinate	Extract	Raffinate
Exp. data				
Col. outlet 5	99.72	94.42	38.38	40.40
Col. outlet 6	99.73	94.97	39.71	41.78
Cal. * No. 5	99.99	98.17	40.29	40.77
RSD, %	0.19	2.75	3.44	0.65
Cal. A * No. 6	99.99	98.22	40.51	40.77
RSD, %	0.36	2.38	1.40	1.73
Cal. B**	99.99	98.21	40.24	40.77
RSD, %	0.19	2.78	3.34	1.73

RSD = Relative standard deviation between experimental and calculated data.
A* = Value calculated with porosity values ϵ_i.
B** = Value calculated with average porosity ϵ_{av}.

the extract stream is almost pure under these experimental conditions. The raffinate purity drops by up to 3% compared to the purity achieved with the more homogenous column set.

There are other possibilities to identify a "defective" column within the SMB unit than by looking at the internal concentration profiles. The outlet stream profiles also reflect the changes in column quality. In this study, the raffinate outlet profile was not affected by the presence of the "defective" column. However, the profile of the extract stream showed significant changes. In Figure 13, the concentration profiles of the extract outlet stream is displayed during a superperiod (eight cycles). Comparing the profiles obtained with the homogeneous column set (dotted line), and those with the "defective" column shows a significant difference. The profiles obtained with the homogeneous set show almost no concentration variations from a switching cycle to the next. The circle in Figure 13 identifies the position of the "defective" column during the duration of

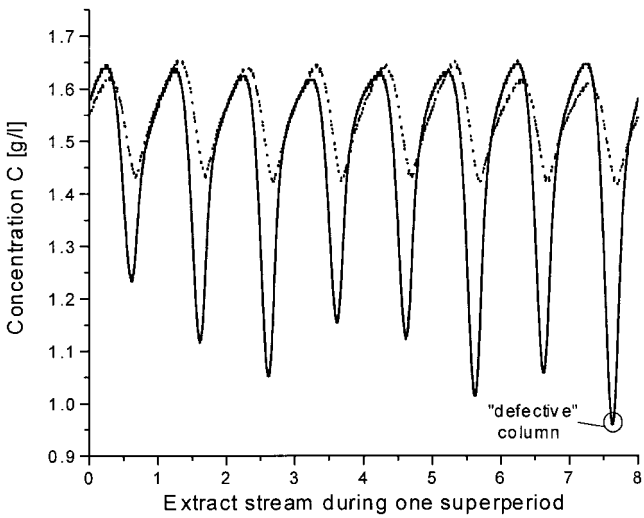

Figure 13. Outlet profiles of the extract stream during one superperiod.

Solid—recorded when detectors at outlet of "defective" column, and dotted—homogenous column set.

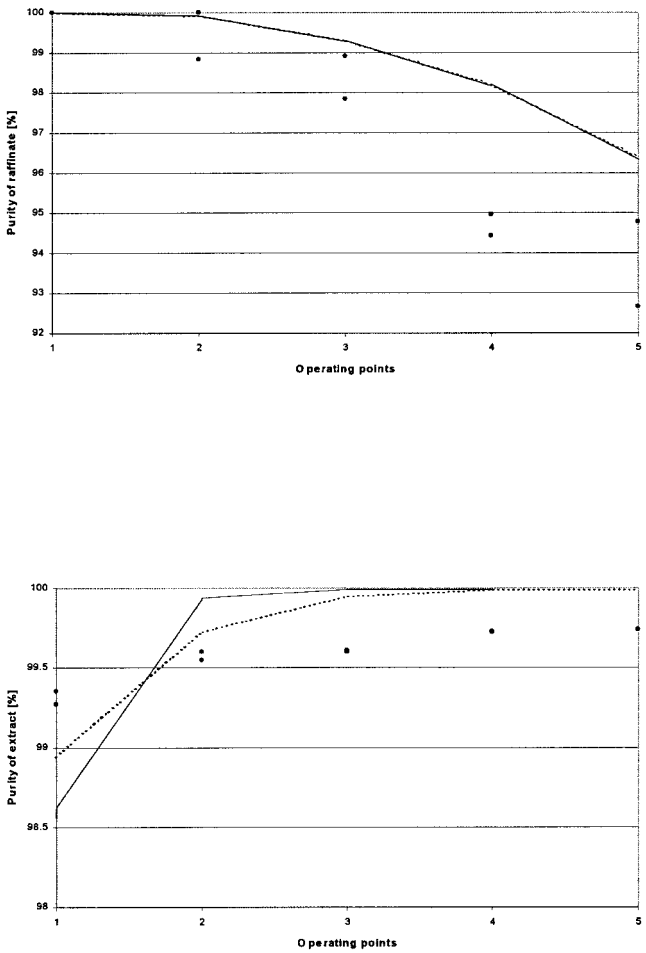

Figure 14. Comparison between experimental and calculated raffinate, and extract purities for operating points op1–5 (Table 3) with one "defective" column.

●—Experimental data, solid line—purity calculated with average porosity ($\epsilon_{av} = 0.648$), and three-layer model (Eqs. 5 and 6), dashed line—purity calculated with average porosity and three-layer model.

the superperiod. Note, however, that changes in the concentration profiles of the outlet stream should not be mistaken for changes in the purity of this stream, as shown in Table 7.

The variations of the purity at the different operating points are displayed in Figure 14 in the case of a "defective" column in the set. The isotherm models give a good agreement between the experimental extract purities, and the values calculated with the average column porosity. By contrast, the purity of the raffinate stream varies more significantly. The variations of the purity calculated for the stream eluting from the "defective" column differ considerably from those resulting from the experimental data.

However, using the information provided by the online detector system, and by the analysis of the outlet streams, provides an excellent tool to identify deviations during the operation of a SMB process. Hence, the operating parameters can be adjusted to take properly into account the performance loss due to the heterogeneity of a set of chromatographic columns, and to guarantee robust operation of an SMB separation.

Conclusions

The results of this detailed study provide an improved understanding of the SMB process and support the initial findings of the authors (Mihlbachler et al., 2001, 2002a). In order to be able to model the behavior correctly of an SMB unit, it is necessary to measure accurately and to model carefully the adsorption isotherms of the feed components in the selected chromatographic system.

In our case, the competitive adsorption of the Tröger's base enantiomers onto the CSP has a very unusual behavior. The more retained enantiomer exhibits an isotherm with an inflection point, which is relatively rare for small molecules, and with enantiomers. By contrast, the less retained enantiomer shows Langmuir adsorption behavior when pure and cooperative interactions with the more retained enantiomer. The principle of the SMB process is based on the formation of sharp fronts at the head of the raffinate band, and also the rear of the extract band. This work demonstrates that the SMB process can be successfully designed for complex adsorption isotherms with an inflection point. It must be emphasized that the use of an online combination of a UV-detector and a polarimeter affords the possibility to monitor the internal concentration profiles of each enantiomer. This information, together with the availability of calculated profiles which are in good agreement with the experimental ones, was a considerable asset in the successful completion of this work.

The influence of the heterogeneity of the column set on the performance of the separation process can now be taken into account when modeling SMB separations. The fact that the true periodicity of a SMB unit is the superperiod had been supported during these theoretical and experimental studies (Mihlbachler et al., 2001, 2002a), especially by the significant variations observed in the SMB output, when the column set is turning around the four sections of the unit. The results reported here demonstrate differences in the calculated performance of the SMB process, as shown in Tables 4–7, and elsewhere in more detail (Mihlbachler, 2002), when implementing the average or the exact column porosity in the model. Other parameters such as the extra-column volumes, and the asymmetric of the SMB design, may also contribute to performance fluctuations during a superperiod. In this study, however, the most influential component that could not be incorporated into the models of adsorption and SMB behavior was the behavior of the impurities present in the feed. They were distributed along the entire chromatographic profile. The achiral cleanup attempts of the sample were successful, but insufficient. Such impurities are common phenomena in pharmaceutical production. The fact that, in spite of the minor troubles due to these impurities, the process that could be modeled successfully gives additional relevance to this study, and shows that it was performed on a realistic separation problem.

Now, the theoretical tools and detector systems are available to predict and to observe the effects of heterogeneity of the column set of the SMB unit, and the complex multilayer adsorption behavior that may be involved in enantioseparations. Both are critical requirements for the successful implementation of computer-assisted method development, and of process-control systems within the SMB unit.

Acknowledgments

This work was supported in part by Grant CHE-00-70548 of the National Science Foundation, and by the cooperative agreement between the University of Tennessee and the Oak Ridge National Laboratory. Additional funding was given by NATO grant OUTRLG971480. The authors are grateful to Chiral Technologies, Inc., for the gift of column and stationary phase, and to PDR Chiral, Inc. for assistance with the polarimeter technology, and to Prochrom for the generous gift of the SMB unit.

Notation

a_i = Henry isotherm coefficient
a_{ik}^* = amount of component i per volume and unit concentration
A = column cross section area, cm^2
b_i = isotherm parameter, cm^3/g
b_{ii} = isotherm parameter Eqs. 6 and 5 $(cm^3/g)^2$
b_{iii} = isotherm parameter Eqs. 5 $(cm^3/g)^3$
C = liquid phase concentration, g/cm^3
D_{ap} = axial dispersion coefficient, cm^2/s
F = phase ratio
L_C = column length, cm
N = theoretical number of plates
P = polynomial
$Prod$ = production rate of component 1 or 2, g/day kg_{pack}
$Pure$ = purity, %
q = solid phase concentration, g/cm^3
q_s = saturation capacity, g/cm^3
Q = flow rate, cm^3/min
r = dimensionless flow rate
t = time, s
t^* = switching time, s
u = liquid phase flow velocity, cm/s
z = axial coordinate

Greek letters

ϵ_k = overall void fraction

Abbreviations

RSD = relative standard deviation, %
SD = standard deviation

Literature Cited

Ahuja, S. *Chiral Separation by Chromatography,* American Chemical Society, Washington, DC, Oxford University Press, New York (2000).

Antos, D., and A. Seidel-Morgenstern, "Application of Gradients in the Simulated Moving Bed Process," *Chem. Eng. Sci.,* **56,** 6667 (2001).

Azevedo, D., L. Pais, and A. Rodrigues, "Enantiomers Separation by Simulated Moving Bed Chromatography. Non-Instantaneous Equilibrium at the Solid-Fluid Interface," *J. Chromatogr. A,* **865,** 187 (1999).

Blümel, C., P. Hugo, and A. Seidel-Morgenstern, "Quantification of Single Solute and Competitive Adsorption Isotherms using a Closed-Loop Perturbation Method," *J. Chromatogr. A,* **827,** 175 (1998).

Cherrak, D., S. Khattabi, and G. Guiochon, "Adsorption Behavior and Prediction of the Band Profiles of the Enantiomers of 3-Chloro-1-Phenyl-1-Propanol Influence of the Mass Transfer Kinetics," *J. Chromatogr. A,* **877,** 109 (2000).

FDA, "FDA Policy Statement for the Development of New Sterioisomeric Drugs," *Chirality,* **4,** 338 (1992).

Fornstedt, T., P. Sajonz, and G. Guiochon, "A Closer Study Of Chiral Retention Mechanisms," *Chirality,* **10,** 375 (1998).

Fricke, J., M. Meuer, J. Dreisörner, and H. Schmidt-Traub, "Effect of Process Parameters on the Performance of a Simulated Moving Bed Chromatographic Reactor," *Chem. Eng. Sci.,* **54,** 1487 (1999).

Grill, C., and L. Miller, "Separation of a Racemic Pharmaceutical Intermediate using Closed-Loop Steady State Recycling," *J. Chromatogr. A,* **827,** 359 (1998).

Guiochon, G., S. G. Shirazi, and A. Katti, *Fundamentals of Nonlinear and Preparative Chromatography,* Academic Press, Boston, MA (1994).

Hill, T., *An Introduction to Statistical Thermodynamics,* Addison-Wellsley, Reading, MA (1960).

Kawase, M., A. Pilgrim, T. Araki, and K. Hashimoto, "Lactosucrose Production using a Simulated Moving Bed Reactor," *Chem. Eng. Sci.,* **56,** 453 (2001).

Khattabi, S., D. Cherrak, K. Mihlbachler, and G. Guiochon, "Enantiomer-separation of 1-Phenyl-1-Propanol by Simulated Moving Bed under Linear and Nonlinear Conditions," *J. Chromatogr. A,* **893,** 307 (2000).

Klatt, K.-U., F. Hanisch, G. Dünnebier, and S. Engell, "Model-Based Optimization and Control of Chromatographic Separation Processes," *Comput. Chem. Eng.,* **24,** 1119 (2000).

Kloppenburg, E., and E. Gilles, "Automatic Control of the Simulated Moving Bed Process for C8 Aromatics Separation using Asymptotically Exact Input/Output-Linearization," *J. Proc. Cont.,* **9,** 41 (1999).

Kniep, H., G. Mann, C. Vogel, and A. Seidel-Morgenstern, "Separation of Enantiomers through Simulated Moving Bed Chromatography," *Chem. Eng. Tech.,* **23,** 853 (2000).

Lin, B., Z. Ma, S. Golshan-Shirazi, and G. Guiochon, "Study of the Representation of Competitive Isotherms and of the Intersection Between Adsorption Isotherms," *J. Chromatogr.,* **475,** 1 (1989).

Lorenz, H., P. Sheehan, and A. Seidel-Morgenstern, "Coupling of Simulated Moving Bed Chromatography and Fractional Crystallisation for Efficient Enantioseparation," *J. Chromatogr. A,* **908,** 201 (2001).

Marteau, P., N. Zanier-Szydlowski, A. Aoufi, G. Hotier, and F. Cansell, "Remote Raman Spectroscopy for Process Control," *Vib. Spectrosc.,* **9,** 101 (1995).

Migliorine, C., M. Fillinger, M. Mazzotti, and M. Morbidelli, "Analysis of Simulated Moving-Bed Reactors," *Chem. Eng. Sci.,* **54,** 2475 (1999).

Mihlbachler, K., *Enantioseparation via SMB Chromatography: A Study of Tröger's Base Unique Adsorption Behavior and the Influence of Heterogeneity of the Column Set on the Performance of the SMB Process,* Logos-Verlag, Berlin, Germany (2002).

Mihlbachler, K., J. Fricke, T. Yun, A. Seidel-Morgenstern, H. Schmidt-Traub, and G. Guiochon, "Effect of Homogeneity of Column Set on the Performance of Simulated Moving Bed Unit, Part I: Theory," *J. Chromatogr. A,* **908,** 49 (2001).

Mihlbachler, K., A. Jupke, A. Seidel-Morgenstern, H. Schmidt-Traub, and G. Guiochon, "Effect of Homogeneity of Column Set on the Performance of Simulated Moving Bed Unit, Part II: Experimental Study," *J. Chromatogr. A,* **944,** 3 (2002a).

Mihlbachler, K., K. Kaczmarski, A. Seidel-Morgenstern, and G. Guiochon, "A Comparison of Adsorption Isotherm Parameters of the Tröger's Base as Determined by Frontal Analysis and the Perturbation Method," *J. Chromatogr. A,* **955,** 35 (2002b).

Nicoud, R.-M., and A. Seidel-Morgenstern, *Isolation and Purification,* **2,** 165 (1996).

Pais, L., J. Loureiro, and A. Rodrigues, "Modeling Strategies for Enantiomers Separation by SMB Chromatography," *Sep. Purif. Technol.,* **20,** 67 (2000).

Pedeferri, M., G. Zenoni, M. Mazzotti, and M. Morbidelli, "Experimental Analysis of a Chiral Separation Through Simulated Moving Bed Chromatography," *Chem. Eng. Sci.,* **54,** 3735 (1999).

Rouchon, P., M. Schonauer, P. Valentin, and G. Guiochon, "Numerical Simulation of Band Propagation in Nonlinear Chromatography," *Sep. Sci. Technol.,* **22,** 1793 (1987).

Ruthven, D., and C. Ching, "Counter-Current and Simulated Moving Bed Adsorption Separation Processes," *Chem. Eng. Sci.,* **44,** 1011 (1989).

Seidel-Morgenstern, A., C. Blümel, and H. Kniep, "Efficient Design of the SMB Process Based on a Perturbation Method to Measure Adsorption Isotherms and on a Rapid Solution of the Dispersion Model," *Fundamentals of Adsorption,* 6th ed., F. Meunier, ed., Elsevier, Amsterdam, p. 303 (1998).

Seidel-Morgerstern, A., and G. Guiochon, "Modeling of the Competitive Isotherms and the Chromatographic Separation of Two Enantiomers," *Chem. Eng. Sci.,* **48,** 2787 (1993a).

Seidel-Morgerstern, A., and G. Guiochon, "Thermodynamics of the Adsorption of Troger's Base Enantiomers from Ethanol on Celluce Triacetate," *J. Chromatogr. A,* **631,** 37 (1993b).

Stanley, B., C. Foster, and G. Guiochon, "On the Reproducibility of Column Efficiency in High Performance Liquid Chromatography and the Role of the Packing Density," *J. Chromatogr. A,* **761,** 41 (1996).

Storti, G., M. Masi, S. Carra, and M. Morbidelli, "Optimal Design of Multicomponent Countercurrent Adsorption Separation Processes Involving Nonlinear Equilibria," *Chem. Eng. Sci.,* **44,** 1329 (1989).

Storti, G., M. Mazotti, M. Morbidelli, and S. Carra, "Robust Design of Binary Countercurrent Adsorption Separation Processes," *AIChE J.,* **39,** 471 (1993).
Thiele, A., T. Falk, L. Tobiska, and A. Seidel-Morgenstern, "Prediction of Elution Profiles in Annular Chromatography," *Comput. Chem. Eng.,* **25,** 1089 (2001).
Uretschläger, A., A. Einhauer, and A. Jungbauer, "Continuous Separation of Green Fluorescent Protein by Annular Chromatography," *J. Chromatogr. A,* **908,** 243 (2001).
Wu, D.-J., Z. Ma, and N.-H. Wang, "Optimization ot Throughput and Desorbent Consumption in Simulated Moving-Bed Chromatography for Paclitaxel Purification," *J. Chromatogr. A,* **855,** 71 (1999).
Zenoni, G., M. Pedeferri, M. Mazzotti, and M. Morbidelli, "On-line Monitoring of Enantiomer Concentration in Chiral Simulated Moving Bed Chromatography," *J. Chromatogr. A,* **888,** 73 (2000).
Zhong, G., and G. Guiochon, "Analytical Solution for the Linear Ideal Model of Simulated Moving Bed Chromatography," *Chem. Eng. Sci.,* **51,** 4307 (1996).

Manuscript received Feb. 5, 2003, and revision received July 2, 2003.